Research Article

Tuning the electronic, optical and structural properties of GaS/C_2N van der Waals heterostructure for photovoltaic application: first-principle calculations

Seiso Emmanuel Tsoeu[1] · Francis Opoku[1] · Penny Poomani Govender[1]

Received: 22 November 2019 / Accepted: 21 January 2020 / Published online: 4 February 2020

Abstract
Due to the increased energy demand, a large amount of renewable energy is required to sustain the lives of people. The visible light semiconductors for photovoltaic cells with optical properties and a tunable bandgap have been studied to bring the solution to energy crises. Two-dimensional (2D) semiconductors including gallium sulphide (GaS) and carbon nitride (C_2N) monolayers as a photovoltaic material were investigated by designing GaS/C_2N van der Waals (vdWs) heterostructure. In this study, density functional theory (DFT) was employed to study the structural, photovoltaic applications, electronic and optical properties of GaS/C_2N vdWs heterostructure. In comparison with the counterparts of GaS and C_2N monolayers, the GaS/C_2N vdWs heterostructure showed a lower desirable direct bandgap of 1.251 eV and the projected density of states shows a type-I band alignment. The work function of the heterostructure is much lesser than the GaS monolayer and C_2N layer, which signifies that less energy will be needed for electrons to transfer from the ground state. The charge density transfer shows charge redistribution from GaS to C_2N. The power conversion efficiency (η) of GaS/C_2N heterostructure is calculated to be 17.8%. Based on the results, the 2D GaS/C_2N heterostructure is predicted to be effective material in developing a high-performance photovoltaic device for future use.

Keywords Photovoltaic cells · Density functional theory · Heterostructure · Power conversion efficiency

1 Introduction

As the energy crisis is continuously increasing globally, the demand for sufficient energy is of high interest. The technique of using fossil fuels to harvest energy has led to very severe environmental issues, such as air pollution. The burning of fossil fuels releases greenhouse gases, such as carbon dioxide (CO_2) [1], sulphur dioxide (SO_2) [2], and others [3, 4]. Since fossil fuels are non-renewable resources, they will not be available in future, as they will be used up or fade out due to their toxic nature. This has led to the investigation of a photovoltaic (PV) cell as the ideal solution. The PV method has been a clean, eco-friendly, reliable and safe way of producing energy.

In the early years, titanium oxide (TiO_2) monocrystalline was used in PV cells to harvest solar energy, where TiO_2 had percentage conversion efficiency (PCE) of about 3.8% [5]. When TiO_2 was later incorporated in the flat zinc oxide (ZnO) through the deposition process by aerosol spray pyrolysis, the large conversion efficiency of about 15.0% was observed [6, 7]. This shows its great potential as a new photovoltaic technology [6, 7]. Due to the above-mentioned improvement, more work has been done with PCE of over 22.0% [8–10] and they are cost-effective and cause no harm to the environment and human health.

Graphene, a single layer consisting of carbon atoms arranged in a hexagonal lattice form, has brought a lot of attention in energy production [11] because of its

✉ Francis Opoku, ofrancis2010@gmail.com; ✉ Penny Poomani Govender, pennyg@uj.ac.za | [1]Department of Chemical Sciences, University of Johannesburg, P. O. Box 17011, Doornfontein Campus, Johannesburg 2028, South Africa.

remarkable magnetic and electronic properties [12]. Two-dimensional (2D) materials have shown a wide application in the photovoltaic cell [13, 14] and photocatalysis [15]. With their promising physical and chemical properties for future applications in solar cells, nanoelectronic and nano-optoelectronics devices, and 2D transition metal dichalcogenides (TMDs) are gaining much attention [16–18]. Up to now, various 2D materials, such as g-C_3N_4, C_2N, C_3N_4 and C_6N_6 [19–21], as well as dichalcogenides metals [22], phosphorus [23], silicene [23, 24] and others, have been broadly used in experimental and theoretical studies for application in photovoltaic cells [25], electronic devices [26] and others [27].

The carbon nitride (C_2N) material, which contains pore and nitrogen atoms, has been successfully synthesised with a bottom-up wet-chemical reaction method [20] with a bandgap energy of ~ 1.96 eV [28–30]. Theoretical reports predict that the band edge positions and the bandgap of C_2N sheet can be tuned by changing their layer number, external electric field and stacking order with promising high-performance photovoltaic properties [31]. C_2N sheet contains benzene rings that are been bridged by the pyrazine rings, having a six-membered D_{2h} ring with the two nitrogen atoms facing each other [29]. The phonon modes of C_2N monolayer are close to graphene; this suggests that C_2N can have high structural stability, which can be useful to generate high energy for photovoltaic cell [32].

As a field-effect transistor device, C_2N shows a 10^7 on/off ratio that is higher than that of graphene [30]. Unlike other 2D semiconductor materials, C_2N is low cost and easy to be synthesised [33]. These properties make it a more promising material for applications in a photovoltaic cell and nanoelectronic and nano-optoelectronics devices [34–36]. The distributions of charges from the valence band maximum (VBM) to conduction band minimum (CBM) states are not well separated, which can reduce the absorbing efficiency of light due to the fast recombination of photogenerated electrons and holes [37]. Nevertheless, to improve the performance of C_2N as a photovoltaic cell, usually, the electronic structure of the 2D materials should be coupled with other 2D materials [38]. The 2D van der Waals (vdWs) heterostructure materials are used to improve the absorption of solar energy in PV cells in order to generate efficient energy that can be converted into direct electrical energy.

Recently, several studies have shown that suitable bandgap structures and well efficient charge separation are important in achieving an efficient photovoltaic device [39]. In a photovoltaic cell, electron–hole pairs are separated when visible light irradiates on the semiconductor surface, where electrons (e^-) will be promoted to the n-type and holes (e^+) will be on the p-type [40]. However, there is still high rapid recombination of charge carriers in C_2N. Lately, vdWs heterostructure has been an efficient way of adjusting the properties of 2D materials, such as band structure tuning and charge carrier separation [41]. Type-I (symmetric), type II (staggered) and type III (broken) band alignments in vdW heterostructures have their own specific applications to allow various device varieties [42–45]. To enhance the effective charge separation of C_2N nanosheet, the GaS monolayer is coupled with C_2N nanosheet [46]. GaS is a semiconductor with an indirect bandgap of 2.59 eV [47]. A GaS semiconductor is considered as a promising material, close to blue light-emitting devices [46]. Furthermore, it has the ability to emit in both photoluminescence and electroluminescence regions [48, 49] because they both give an insight into carrier dynamics and lateral relation to reducing electron–hole pairs recombination [50].

In this paper, we investigate a GaS/C_2N vdW heterostructure as a photovoltaic cell using density functional theory (DFT) calculations. The DFT calculations are based on geometry optimisation, the total projected density of states, charge population analysis, optical properties as well as power conversion efficiency. Moreover, the band structure properties are predicted, which are more critical in designing new photovoltaic cells. The theoretical results will offer insights into designing other 2D-based photovoltaic materials.

2 Computational details

In this study, first-principle calculations of GaS/C_2N heterostructure and the individual components are performed by means of plane-wave DFT method as implemented in the Cambridge Serial Total Energy Package (CASTEP) code [51] of Material Studio 2016 [52]. The generalised gradient approximation (GGA) with Perdew–Burke–Ernzerhof (PBE) is used to define the exchange-correlation effect [53]. The plane-wave kinetic energy cut-off is set to be 400 eV. The geometry structures are well relaxed until the energy converged to 10^{-6} eV, where the maximum force of atoms is set to be 0.3 eV/Å, maximum stress to be 0.5 GPa and the maximum displacement of the atoms to be 0.01 Å. The vdWs corrections in GaS/C_2N heterostructure and the monolayers were treated by applying DFT-D2 method of Grimme [54]. This method has been demonstrated to give a reliable description of the vdW heterostructures [55, 56]. The electronic configurations of C ($2s^2\ 2p^2$), S ($3s^2\ 3p^4$) and Ga ($3d^{10}\ 4s^2\ 4p^1$) are treated as the valence electrons. In addition, the hybrid Heyd–Scuseria–Ernzerhof (HSE06) [57] functional was used in order to get the accurate electronic properties since GGA-PBE functional underestimates the bandgap energy of most semiconductors [57]. The Brillouin zone is sampled using Monkhorst-Pack

k-point grid of 5 × 5 × 1 for GaS monolayer and 2 × 2 × 1 for C_2N monolayer, and GaS/C_2N heterostructure was used for the calculation of structural relaxation and electronic properties. To avoid artificial interactions, the two layers are constructed with a large vacuum space of about 20 Å.

3 Results and discussion

3.1 Geometry structures

To gain more knowledge of the proposed 2D semiconductors, we first study the geometry structure and electronic properties of the individual materials. The composite structures of C_2N and GaS are shown in Fig. 1.

The primitive unit cell of C_2N sheets consists of 12 carbon atoms and 6 nitrogen atoms with existing uniform holes. The calculated optimised lattice constants of C_2N sheet and GaS monolayer are $a = 8.33$ and 3.57 Å (see Table 1), respectively, as compared to the previous studies of 8.32 and 3.58 Å [58, 59].

Also, the bond lengths of C–N (1.34 Å), C–C_1 (1.43 Å), C–C_2 (1.47 Å) consistently agreed with earlier reported bond lengths 1.34, 1.43 and 1.47 Å [33, 60, 61], respectively. The bond angle of 117.7° for C–N–C slightly deviates from that obtained by Liang et al. [62]. The obtained bond length is 2.43 Å for Ga–S, whereas for Ga–Ga is 2.54 Å, which also agree very well with previous studies [63] of 2.327 and 2.451 Å for G–-S and Ga–Ga, respectively.

In order to avoid high lattice mismatch of the heterostructure, the well-stacking sheets of 3 × 3 of C_2N and 7 × 7 for GaS supercells were used to get 0.30% lattice mismatch, which is desirable to produce the vdW heterostructure. The lattice mismatch (LM) is calculated using Eq. (1):

Table 1 The lattice parameter, binding energy (E_b) and interface distance (d) for C_2N, GaS and GaS/C_2N

Semiconductors	a	b	c	E_b (meV)	d (Å)
	Lattice parameters (Å)				
C_2N	8.33	8.33	27.00	–	–
GaS	3.57	3.57	24.67	–	–
GaS/C_2N	25.75	25.75	28.45	−0.069	3.345

$$\mathrm{LM} = \left(\frac{b-a}{a}\right) \times 100 \tag{1}$$

where a and b are the lattice constants for C_2N sheet and GaS monolayers, respectively. The supercell contains 354 atoms (108 C, 54 N, 30 Ga and 30 S).

The top and side views of the optimised GaS/C_2N heterostructure are shown in Fig. 1a and b, respectively. The optimised geometry of C_2N sheet still sustains its unique planar structure without much distortion, while GaS monolayer remains its linear structure. The lattice parameters of GaS/C_2N heterostructure are $a = b = 25.75$ (Table 1). The equilibrium distance between the optimised structures of C_2N sheet and GaS monolayer is measured as 3.345 Å (Table 1), which agrees with C_2N bilayer with stacking order (3.280 Å) [30]. In order to check the stability between the C_2N sheet and GaS monolayer, the binding energy is calculated, where the two semiconductors are aligned vertically to each other. The binding energy of the heterostructure is calculated according to the following equation [64]:

$$E_b = E_{\mathrm{GaS/C_2N}} - E_{\mathrm{GaS}} - E_{\mathrm{C_2N}} \tag{2}$$

where $E_{\mathrm{GaS/C_2N}}$, E_{GaS} and $E_{\mathrm{C_2N}}$ are the total energies of the relaxed GaS/C_2N heterostructure, GaS monolayer and C_2N

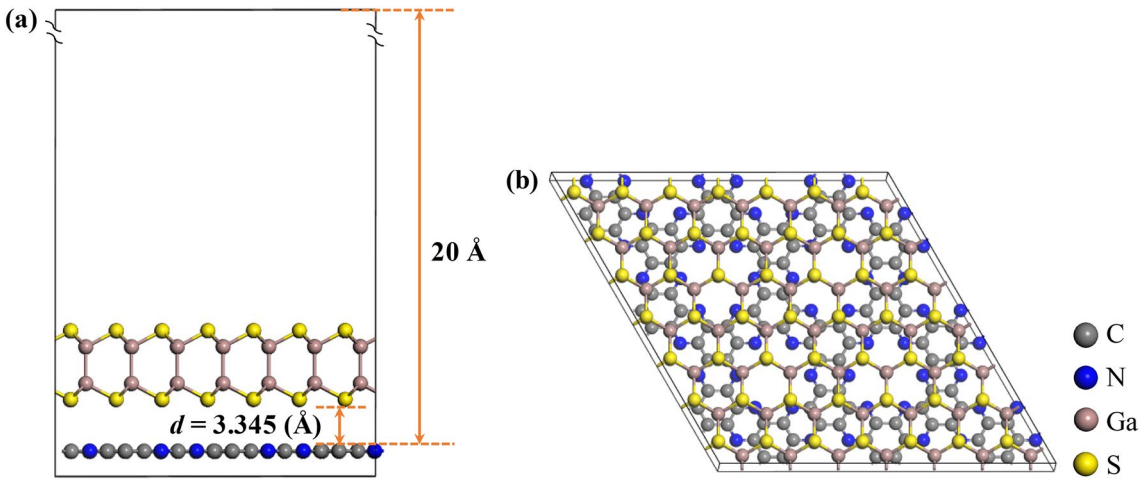

Fig. 1 **a** Side and **b** top views of GaS/C_2N heterostructure

sheet, respectively. An E_b value of − 0.069 meV was calculated; this suggests that C_2N/GaS heterostructure is energetically favourable.

3.2 Electronic properties

The band structures of C_2N sheet, GaS monolayer and GaS/C_2N heterostructure are calculated in order to explore their photovoltaic performance. Moreover, the projected density of state (PDOS) is evaluated to further gain insight into the electronic structural interface and classification of the nature of orbital. The results of the band structures and PDOS are shown in Figs. 2 and 3, respectively.

Generally, C_2N sheet band edges in Fig. 3a are dominated by the C 2*p* and N 2*p* states [39]. The CBM and VBM are both positioned at the *G* point, which makes C_2N monolayer a direct bandgap semiconductor with a bandgap (E_g) energy of 1.96 eV, and this is in good agreement with previous theoretical studies [65]. For GaS monolayer, we observed an indirect bandgap of about 2.38 eV (Fig. 2b), which is close to the experimental value 2.59 eV [47] with a difference of about 0.21 eV. The potential density of state (PDOS) confirms that Ga 4*p* and S 3*p* states dominate the CBM of GaS monolayer, see Fig. 3b. The CBM for GaS is situated between the *Y*–*G* points, while the VBM is at *G* point. The VBM and CBM of GaS are mostly contributed by S 3*p* state.

The bandgap of C_2N and GaS was greatly reduced by forming a heterostructure. The light-harvesting heterostructure with 1.2–1.4 eV narrow bandgap has the supreme efficiency according to the Shockley–Queisser limits [66]; therefore, the reduced bandgap energies of C_2N nanosheet and GaS monolayer can be useful in enhancing the light absorption for solar cells. The indirect bandgap of heterostructure has fundamental importance to its optoelectronic application [67]. This indirect bandgap favours optical transition with significant changes in the wave vector, which can improve the visible light response. The photoexcited charge carriers of an indirect gap semiconductor undergo a change in their momentum state

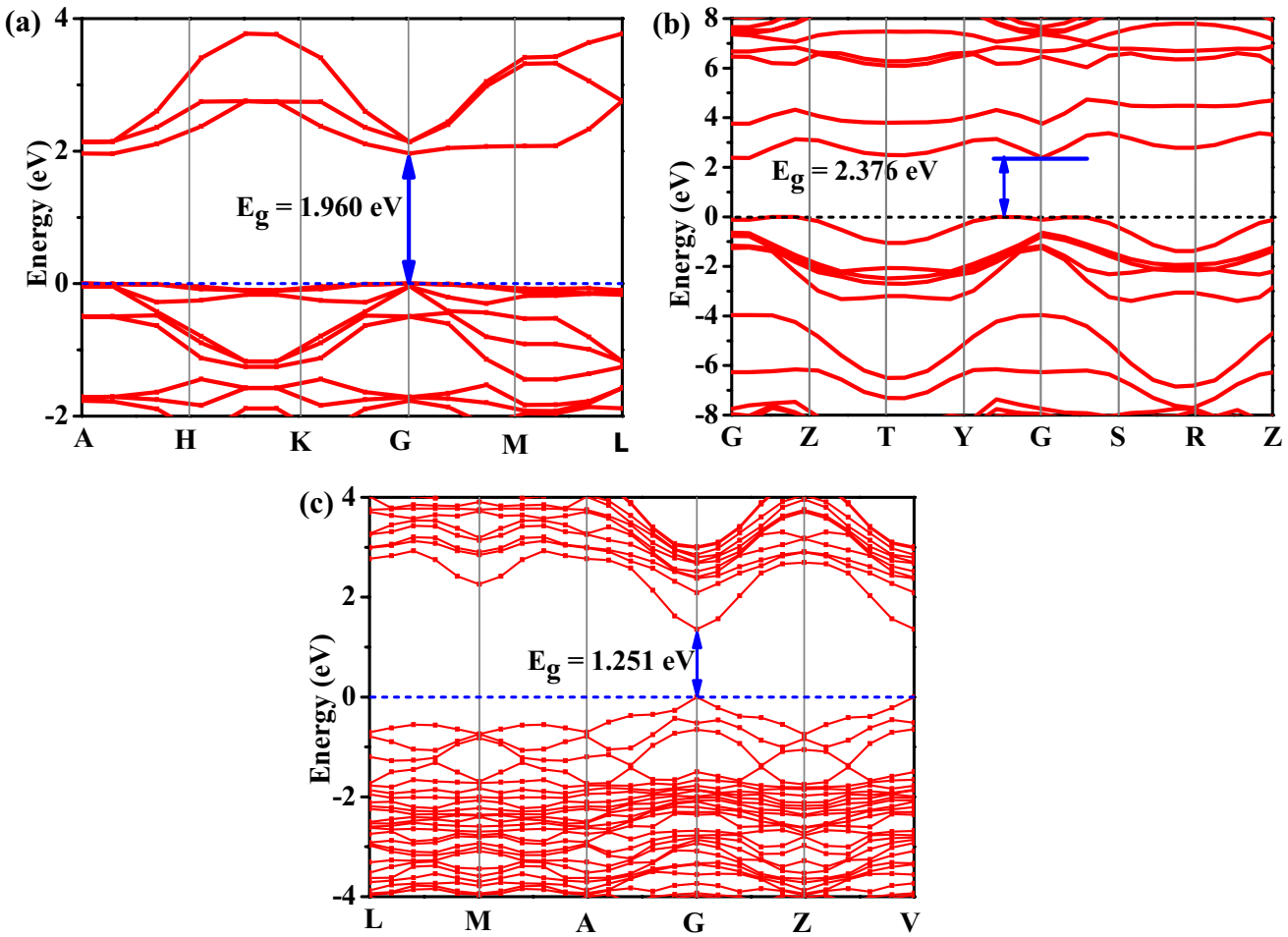

Fig. 2 The calculated HSE06 band structures of **a** C_2N layer, **b** GaS monolayer and **c** GaS/C_2N heterostructure

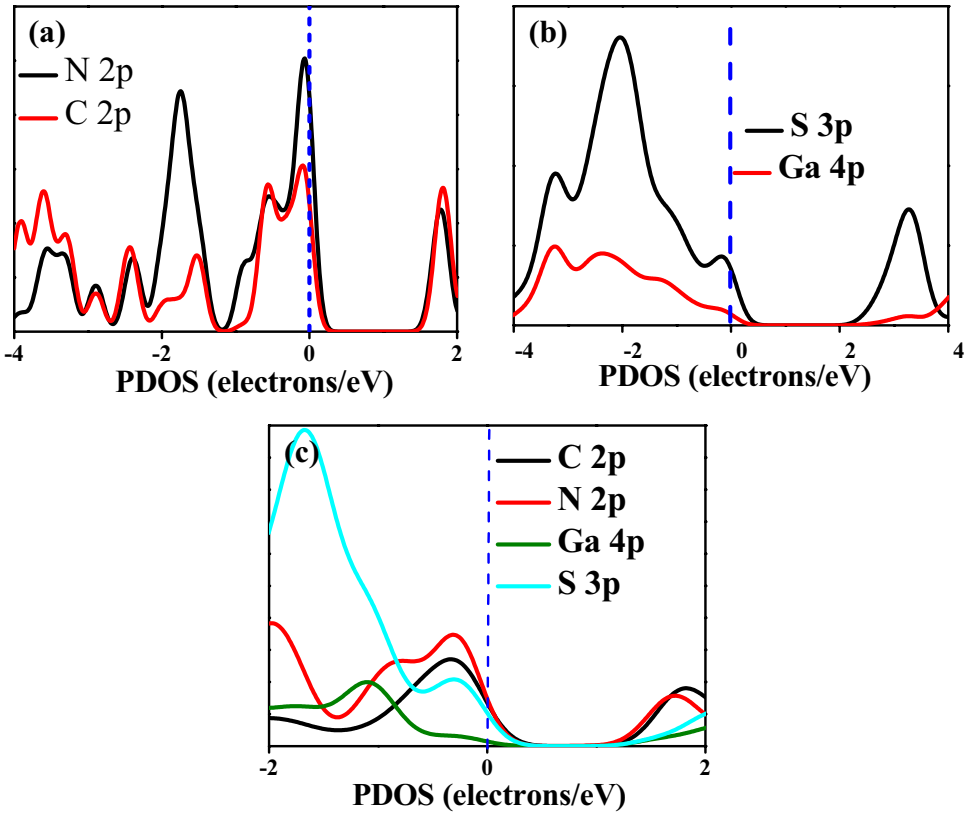

Fig. 3 The calculated HSE06 projected density of state of **a** C_2N layer, **b** GaS monolayer and **c** GaS/C_2N heterostructure

before recombination due to the occurrence of phonon emission [68]. The direct electronic bandgap of GaS/C_2N vdW heterostructure (1.25 eV) in Fig. 2c falls within the range of 1.1–1.5 eV, which is the best bandgap range for PV cells [47, 69, 70]; therefore, the bandgap can lead to efficient absorption of visible light. While the optical transitions through the direct bandgap nature of a heterostructure are recommended, thus, the materials are efficient light emitters for photovoltaic cells [71]. The band alignment properties of C_2N sheet and GaS monolayer form a type-I heterostructure. As the GaS/C_2N heterostructure is exposed to the visible light region, the electrons are photoexcited from the VBM of C_2N sheet. The photogenerated electrons of the GaS monolayer can move well to the CB of the C_2N sheet.

3.3 Work function

Another factor that affects the properties of improving the solar cells is the energy level, and it is well investigated by calculating the work function (Φ) of the individual monolayers and the GaS/C_2N heterostructure. The surface conditions of every material can easily affect the work function, which results from altering the surface electric field induced by the distribution of electrons at the interface [72]. The work function is the amount of energy required to remove an electron from the Fermi level surface of a solid vacuum at an absolute zero. The work function along the *Z* axis is calculated by aligning the Fermi energy level with reference to the vacuum energy level [73].

$$\Phi = E_{\text{vacuum}} - E_{\text{Fermi}} \tag{3}$$

where E_{vacuum} and E_{Fermi} are the energy of an electron at the stationary point in the vacuum in line with the surface and Fermi level, respectively.

The work function for GaS monolayer, C_2N sheet and GaS/C_2N heterostructure is estimated to be 5.79, 6.04 and 5.65 eV, respectively, see Fig. 4.

The calculated work function of GaS monolayer and C_2N sheets shows reduced energy as compared to the reported theoretical results of 6.10 eV for GaS monolayer and 6.18 eV for C_2N sheets [74, 75], which is about 0.314 and 0.140 eV difference between GaS monolayer and C_2N sheet, respectively. The GaS monolayer seems to have a lower work function than the C_2N sheet due to the lower ionisation energy of the S atom as compared to N atom [76]. Therefore, the GaS monolayer that has a lower work function will determine the charge transfer at the interface. The electrons will move from GaS monolayer to C_2N sheet with a low work function potential. In this case, the C_2N sheet will be negatively charged, while GaS will be positively charged due to the high electrostatic induction.

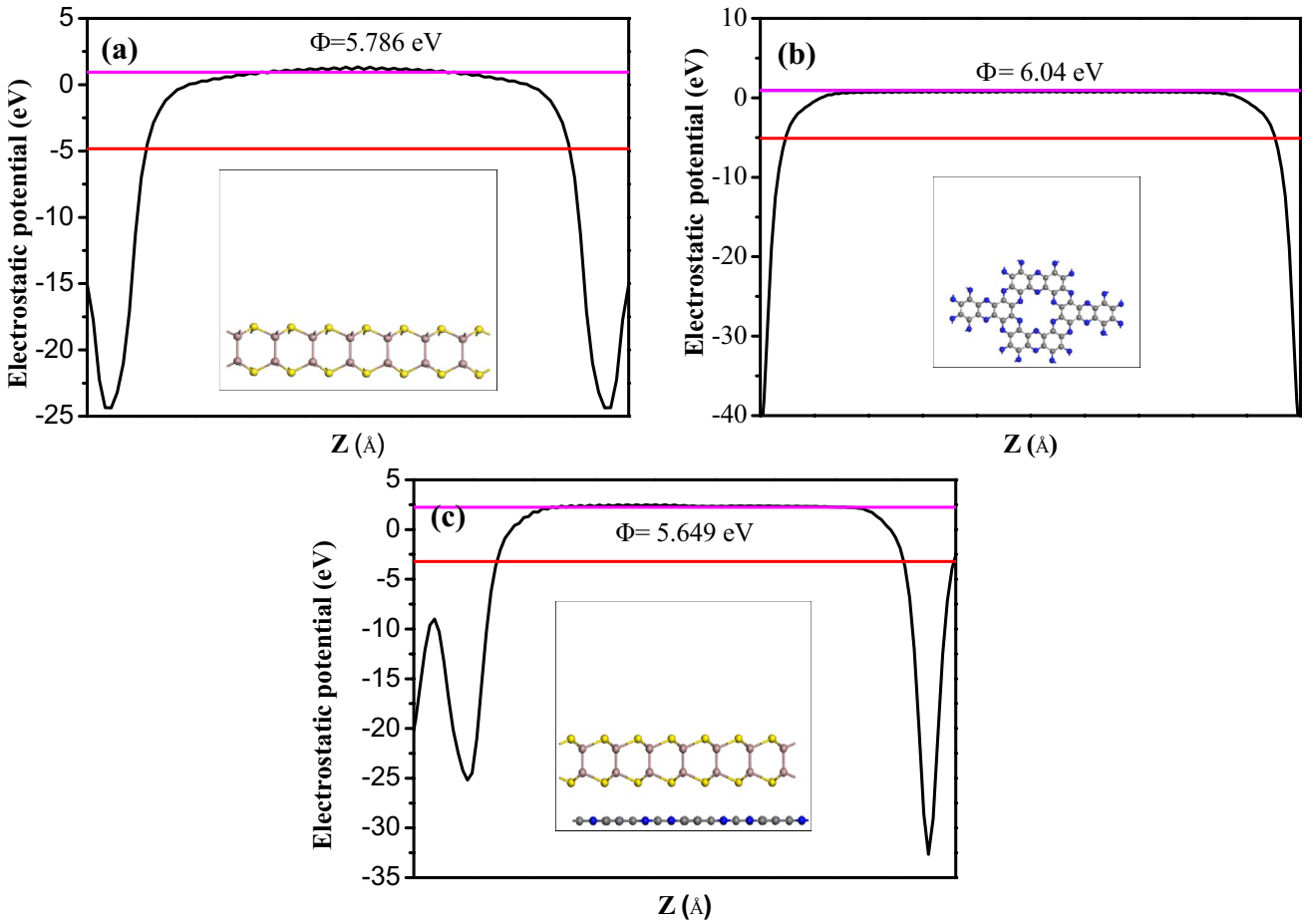

Fig. 4 The calculated work function for **a** GaS monolayer, **b** C_2N sheet and **c** GaS/C_2N heterostructure

The work function of the heterostructure is shown to be decreased from the two monolayers to 5.83 eV due to the efficient interfacial formation of interface and charge transfer [77]. The low work function clearly means that less of energy will be needed to dislodge electrons from the VBM to CBM edges; thus, more electrons will be transferred and the associated phenomenon is that the work function is directly proportional to the kinetic energy gained of an electron. In addition, the electrostatic potential difference at the interface of the GaS/C_2N heterostructure can successfully reduce the charge carrier recombination rate and increase the transfer and separation of the induced charge carriers, which can enhance the power conversion efficiency.

3.4 Charge density difference

The interactions between the two monolayers (C_2N sheet and GaS monolayer) signify the charge distribution between the semiconductors. To further understand the charge transfer of GaS/C_2N heterostructure, a three-dimensional (3D) charger density difference is evaluated with an isosurface valued of 0.003 e/Å^3, where GaS monolayer indicates a substantial charge transfer and separations of electrons after coupled with C_2N sheet, as shown in Fig. 5.

Moreover, high charge accumulation is found on the C_2N sheet surface, consequentially becoming electron-rich surface, whereas the depletion occurred at the GaS monolayer surface, becoming a hole-rich region. The red region predicts that the electron-rich GaS can, therefore, expected to transfer electrons from the GaS monolayer surface to the C_2N sheet surface. Subsequently, GaS monolayer acts as a photosensitiser in GaS/C_2N heterostructure. Therefore, this improves the interaction of strong charge distribution within individual constituent and signifies the separation of electron–hole pairs within the GaS/C_2N heterostructure. This demonstrates the enhancement mechanism of photovoltaic performance of the individual monolayers to form GaS/C_2N heterostructure. The Mulliken charge population analysis shows that the total amount of charge transferred at the GaS/C_2N heterostructure

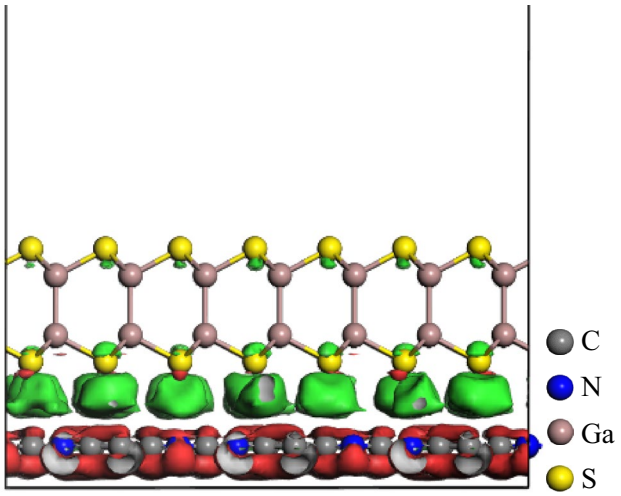

Fig. 5 The 3D charge density difference for GaS/C_2N side view heterostructure. The red and green region represents charge accumulation and depletion, respectively

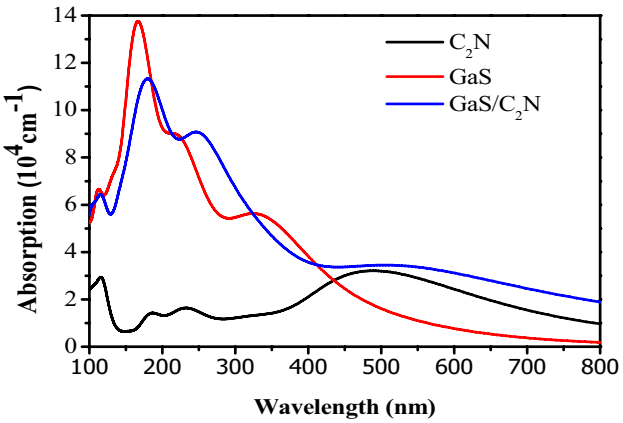

Fig. 6 The calculated light absorption spectrum of a GaS monolayer, C_2N sheet and GaS/C_2N heterostructure

interface is 0.13 |*e*|. The S atoms have an average contribution of − 0.43 |*e*|. Notwithstanding, GaS monolayer makes a contribution of − 0.02 |*e*|; therefore, C_2N monolayer receives an average of 0.13 |*e*|, whereas N is the one that receives more electrons with an average of − 0.31 |*e*|. This charge distribution at the interface may tune the electrostatic potential to enhance solar light detection and harvesting. This charge transfer at GaS/C_2N heterostructure interface indicates that the formation can achieve strong orbital overlapping, leading to highly efficient electron transfer for photovoltaic performance.

3.5 Optical properties

A promising photovoltaic material should absorb as much visible light in order to achieve an efficient electric current conversion. Thus, the optical property of the GaS monolayer, C_2N sheet and GaS/C_2N heterostructure is studied through UV–visible light absorption spectrum. The redshift of the absorption of GaS/C_2N heterostructure was further enhanced in the visible region because of the reduced indirect bandgap when compared to C_2N and GaS counterparts, as shown in Fig. 6.

Thus, comparing GaS monolayer and C_2N sheet, the absorption edges move to the broader wavelength region for GaS/C_2N heterostructure due to the coupled GaS monolayer and C_2N sheet. The outcomes can be comparable to many bandgap semiconductors with very poor visible light absorption capacity [78, 79], where GaS/C_2N heterostructure showed a more absorption intensity in the wide range of 410–800 nm. In this study, the results clearly predicted that the optical properties and the stability of GaS/C_2N heterostructure can enhance the visible light absorption and can be used in photovoltaic devices for conversion of solar light to electrical current. It can be concluded that the GaS/C_2N heterostructure indeed could be used as a photovoltaic material.

For any newly formed semiconductor to be considered as valuable for photovoltaic activity, ideally, the bandgap must be within 1.1–1.5 eV range to enhance the solar absorption energy. Effective charge separation and optical absorption are also influential in photovoltaic performance [80]. Based on the obtained optical absorption results, there is a promising enhancement for visible light for the photovoltaic activity of GaS/C_2N heterostructure as compared to the individual materials. The improved photovoltaic activity affected by the efficient separation and transfer of photogenerated electrons depends heavily on the band structures of the individual parts [81]. The GaS/C_2N heterostructure is assessed by analysing the band position of the valence band and conduction band in relation to the photoexcited electrons of the formed heterostructure. The VBM and CBM of GaS/C_2N heterostructure are evaluated from the respective bandgaps of the individual components and their absolute electronegativity of atoms using the empirical equations:

$$E_{VB} = X - E_e + 0.5E_g \tag{4}$$

$$E_{CB} = E_{VB} - E_g \tag{5}$$

where X is the standard electrode potential ($\simeq$ 4.5 eV), E_e represents the energy of free electrons of the hydrogen scale, and E_g is the estimated bandgap of the studied semiconductor. E_{VB} and E_{CB} represent the conduction band and valence band edge potentials. The X values of C, N, Ga and S are 6.27, 7.30, 3.20 and 6.22 eV, respectively [82]. The X values of C_2N sheet and GaS monolayer are calculated as 4.51 and 4.46 eV, respectively. Therefore, the E_{VB} and E_{CB}

are calculated as 0.99 and − 0.97 eV for C_2N, respectively. In addition, the corresponding band edges of GaS are calculated as 1.15 and − 1.23 eV, respectively. This clearly shows that the CB and VB of GaS are higher than those of C_2N.

3.6 Charge carrier mechanism

Based on the band edges results, the possible reaction and transfer of energised electrons are proposed for GaS/C_2N heterostructure, as shown in Fig. 7.

The photoexcited electrons and holes in the CB and VB, respectively, of the GaS monolayer, can be easily transferred to C_2N sheet. The mechanism in Fig. 7 further confirms the type-I heterostructure formation with CB and VB of C_2N sheet which is lower than that of GaS monolayer. The type-I band alignment of GaS/C_2N heterostructure signifies that the formation can yield better improvement of sunlight and transfer of charge carriers [83].

4 Power conversion efficiency

In the numerical calculations of power conversion efficiency for GaS/C_2N heterostructure based on the obtained bandgap, the maximum open-circuit voltage (V_o), short-circuit current density (J_{sc}) and power conversion efficiency (η) of the formed heterostructure are calculated using Eqs. 7 and 8:

$$qV_{OC} = E_g - E_{loss} \tag{7}$$

The relationship between the variable parameter E_{loss} (adopted with the values of 0.7 eV) [66] and the E_g of the GaS/C_2N heterostructure was used to calculate the maximum open-circuit voltage (qV_{oc}) using the above equation.

The maximum short-circuit current density (J_{sc}) can be used to evaluate the incident photons, where the formed GaS/C_2N heterostructure will generate electron-hole pairs after absorbing the incoming photons. The absorption can only occur if the energy of the incident photons is equal to or larger than the of the formed GaS/C_2N heterostructure. The following equation can be used to calculate J_{sc}

$$J_{SC} = q \int_{E_g}^{\infty} b_s(E)\, dE, \tag{8}$$

where $b_s(E)$ signifies the incident spectral photon flux density and q is the electron charge.

The maximum power conversion efficiency (η) of GaS/C_2N heterostructure is calculated by introducing the total incident power density (P_s) of 100 mW cm^{-2} [84]. The high fill factor (FF) of 0.85 [85] was essentially used to calculate

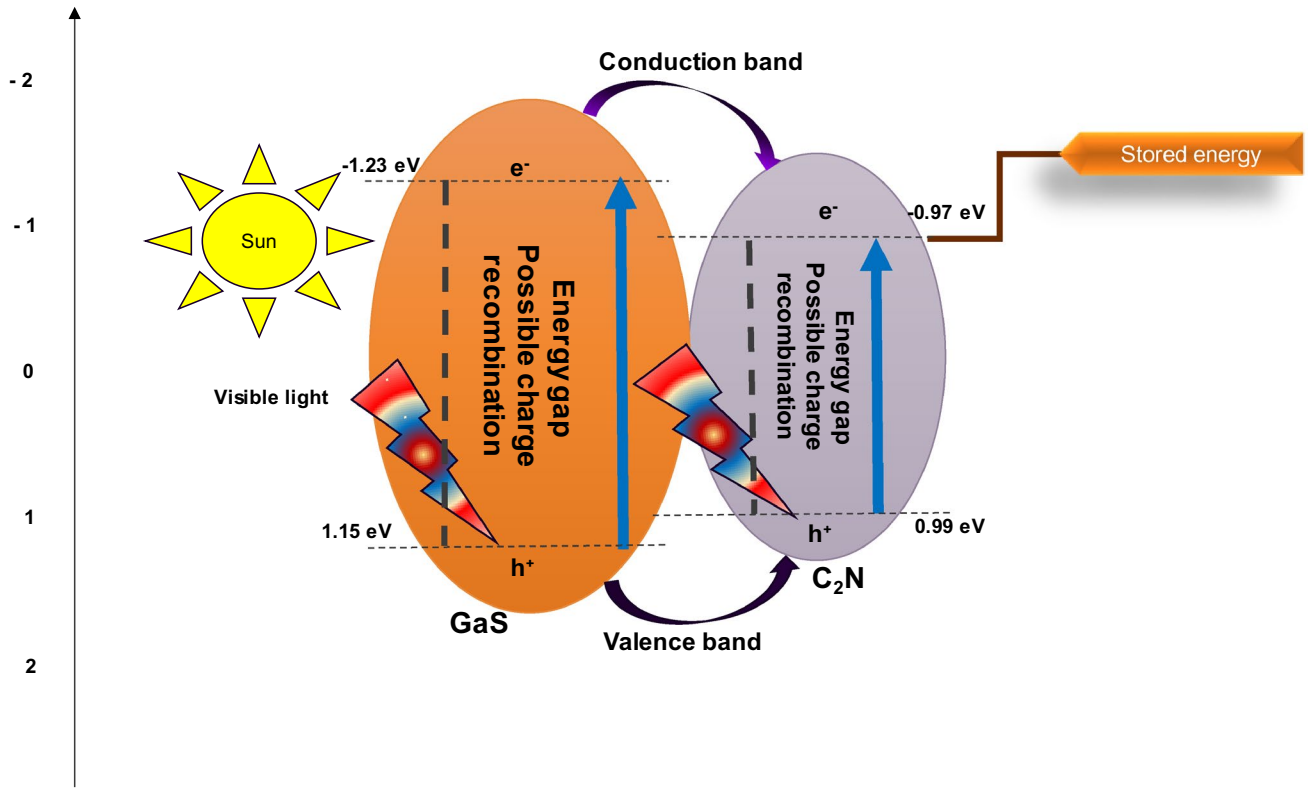

Fig. 7 Band alignment showing the conduction band and valence band of C_2N sheet and GaS monolayer

the PCE of GaS/C_2N heterostructure for PV cells, with a maximum short-circuit current density (J_{sc} of 37.9 mA/cm^{-2}) [86]. The fill factor (FF) is a parameter which, in conjunction with V_{oc} and I_{sc}, determines the maximum power from a solar cell. The FF is defined as the ratio of the maximum power (P_{max}) from the solar cell to the product of V_{oc} and I_{sc}. Graphically, the FF is a measure of the squareness of the solar cell and is also the area of the largest rectangle which will fit in the IV curve. The total incident power density (P_s) is achieved by applying integration normalisation spectral irradiance stated by National Renewable Energy Laboratory (NREL) and is calculated with the following equation:

$$P_s = \int_0^\infty Eb_s(E)\mathrm{d}E \tag{9}$$

Finally, PCE (η) formula is calculated as:

$$\eta = \frac{\mathrm{FF} \cdot J_{SC} \cdot V_{oc}}{P_s} \tag{10}$$

For the 2D GaS/C_2N heterostructure, the excellent electron–hole pairs transport properties, the reduced bandgap, and enhanced optical absorption are more effective in increasing the power conversion efficiency. It is clear that GaS/C_2N heterostructure can improve the photovoltaic performance since both V_{oc} and I_{sc} result in a high PCE of about 17.8%. This suggests that GaS/C_2N heterostructure can be an ideal material to be used in photovoltaic cells.

5 Conclusion

In this study, the first-principle DFT calculations were used to explore the performance of GaS/C_2N heterostructure as a photovoltaic cell. The obtained electronic properties of the heterostructure clearly show a reduced indirect bandgap of 1.251 eV as compared to their individual counterparts. Furthermore, the formed 2D GaS/C_2N heterostructure shows a very strong visible light absorption edge with a lower work function of 5.649 eV. The GaS/C_2N vdWs heterostructure exhibits PCE of 17.8%, which is enhanced by the reduced indirect bandgap and enhanced visible light absorption edge. As a search for lead-free materials, still a major consent in the photovoltaic cells, the results predicted that GaS/C_2N vdWs heterostructure can be a very suitable replacement for leaded materials to reduce the toxicity that it possesses on human health and environment.

Acknowledgements The authors would like to acknowledge the financial contributions from the Faculty of Science: the University of Johannesburg-South Africa, Centre for Nanomaterials and Science Research, Department of Chemical Sciences and the National Research Foundation (TTK14052167682). We acknowledge the computational support provided by the Centre for High-Performance Computing (CHPC), Cape Town.

Compliance with ethical standards

Conflict of interest The authors declare that they have no conflict of interest.

References

1. Tsoutsos T, Frantzeskaki N, Gekas V (2005) Environmental impacts from the solar energy technologies. Energy Policy 33(3):289–296
2. Solangi K, Islam M, Saidur R, Rahim N, Fayaz H (2011) A review on global solar energy policy. Renew Sustain Energy Rev 15(4):2149–2163
3. Bilen K, Ozyurt O, Bakırcı K, Karslı S, Erdogan S, Yılmaz M, Comaklı O (2008) Energy production, consumption, and environmental pollution for sustainable development: a case study in Turkey. Renew Sustain Energy Rev 12(6):1529–1561
4. Barakat MS, Bashter II, Tawfik FS, Nagla TF (2016) Health impacts of routine gaseous releases from nuclear facilities. Eur Acad Res 4(9):7795–7813
5. Kojima A, Teshima K, Shirai Y, Miyasaka T (2009) Organometal halide perovskites as visible-light sensitizers for photovoltaic cells. J Am Chem Soc 131(17):6050–6051
6. Gonzalez-Pedro V, Juarez-Perez EJ, Arsyad W-S, Barea EM, Fabregat-Santiago F, Mora-Sero I, Bisquert J (2014) General working principles of $CH_3NH_3PbX_3$ perovskite solar cells. Nano Lett 14(2):888–893
7. Wang JT-W, Ball JM, Barea EM, Abate A, Alexander-Webber JA, Huang J, Saliba M, Mora-Sero I, Bisquert J, Snaith HJ (2013) Low-temperature processed electron collection layers of graphene/TiO_2 nanocomposites in thin film perovskite solar cells. Nano Lett 14(2):724–730
8. Sun P-P, Li Q-S, Feng S, Li Z-S (2016) Mixed Ge/Pb perovskite light absorbers with an ascendant efficiency explored from theoretical view. Phys Chem Chem Phys 18(21):14408–14418
9. Deng X-Z, Zhao Q-Q, Zhao Y-Q, Cai M-Q (2019) Theoretical study on photoelectric properties of lead-free mixed inorganic perovskite $RbGe_1$-xSn$x$$I_3$. CAP 19(3):279–284
10. Fu H (2019) Review of lead-free halide perovskites as light-absorbers for photovoltaic applications: from materials to solar cells. Sol Energy Mater Sol Cells 193:107–132
11. Novoselov KS, Geim AK, Morozov SV, Jiang D, Zhang Y, Dubonos SV, Grigorieva IV, Firsov AA (2004) Electric field effect in atomically thin carbon films. Science 306(5696):666–669
12. Zhou B, Wang X, Dong S, Zhang K, Mi W (2017) Tunable gap opening and spin polarization of two dimensional graphene/hafnene van der Waals heterostructures. Carbon 120:121–127
13. Roy S, Bermel P (2018) Electronic and optical properties of ultra-thin 2D tungsten disulfide for photovoltaic applications. Sol Energy Mater Sol Cells 174:370–379
14. Mak KF, Lee C, Hone J, Shan J, Heinz TF (2010) Atomically thin MoS_2: a new direct-gap semiconductor. Phys Rev Lett 105(13):136805–136820
15. Ashwin Kishore M, Ravindran P (2017) Tailoring the electronic band gap and band edge positions in the C_2N monolayer by

P and As substitution for photocatalytic water splitting. J Phys Chem C 121(40):22216–22224
16. Guan Z, Ni S, Hu S (2018) Tunable electronic and optical properties of monolayer and multilayer Janus MoSSe as a photocatalyst for solar water splitting: a first-principles study. J Phys Chem C 122(11):6209–6216
17. Sun M, Chou J-P, Yu J, Tang W (2017) Effects of structural imperfection on the electronic properties of graphene/WSe 2 heterostructures. J Mater Chem C 5(39):10383–10390
18. Guan Z, Ni S, Hu S (2017) Band gap opening of graphene by forming a graphene/PtSe2 van der Waals heterojunction. RSC Adv 7(72):45393–45399
19. Wang X, Maeda K, Thomas A, Takanabe K, Xin G, Carlsson JM, Domen K, Antonietti M (2009) A metal-free polymeric photocatalyst for hydrogen production from water under visible light. Nat Mater 8(1):76–80
20. Mahmood J, Lee EK, Jung M, Shin D, Jeon I-Y, Jung S-M, Choi H-J, Seo J-M, Bae S-Y, Sohn S-D (2015) Nitrogenated holey two-dimensional structures. Nat Commun 6:6486–6493
21. Srinivasu K, Modak B, Ghosh SK (2014) Porous graphitic carbon nitride: a possible metal-free photocatalyst for water splitting. J Phys Chem C 118(46):26479–26484
22. Wang QH, Kalantar-Zadeh K, Kis A, Coleman JN, Strano MS (2012) Electronics and optoelectronics of two-dimensional transition metal dichalcogenides. Nat Nanotechnol 7(11):699–712
23. Wang T, Lin Y, Tai C, Sivakumar R, Rai D, Lan C (2008) A novel approach for recycling of kerf loss silicon from cutting slurry waste for solar cell applications. J Cryst Growth 310(15):3403–3406
24. Manshanden P, Geerligs L (2006) Improved phosphorous gettering of multicrystalline silicon. Sol Energy Mater Sol Cells 90(7–8):998–1012
25. Bonaccorso F, Colombo L, Yu G, Stoller M, Tozzini V, Ferrari AC, Ruoff RS, Pellegrini V (2015) Graphene, related two-dimensional crystals, and hybrid systems for energy conversion and storage. Science 347(6217):1246501
26. Kang J, Horzum S, Peeters FM (2015) Heterostructures of graphene and nitrogenated holey graphene: moire pattern and Dirac ring. Phys Rev B 92(19):195419–195428
27. De Vos A (1993) The endoreversible theory of solar energy conversion: a tutorial. Sol Energy Mater Sol Cells 31(1):75–93
28. Chen Z, Zhang R, Yang J (2018) First-principles study on layered C_2N–metal interfaces. Langmuir 34(8):2647–2653
29. Kishore MA, Ravindran P (2017) Enhanced photocatalytic water splitting in a C2N monolayer by C-site isoelectronic substitution. Chem Phys Chem 18(12):1526–1532
30. Guan Z, Ni S (2017) Insights from first principles graphene/gC_2N bilayer: gap opening, enhanced visible light response and electrical field tuning band structure. Appl Phys A 123(11):678–686
31. Chetia TR, Ansari MS, Qureshi M (2016) Graphitic carbon nitride as a photovoltaic booster in quantum dot sensitized solar cells: a synergistic approach for enhanced charge separation and injection. J Mater Chem A 4(15):5528–5541
32. Sahin H (2015) Structural and phononic characteristics of nitrogenated holey graphene. Phys Rev B 92(8):085421–085426
33. Guan Z, Lian C-S, Hu S, Ni S, Li J, Duan W (2017) Tunable structural, electronic, and optical properties of layered two-dimensional C_2N and MoS_2 van der waals heterostructure as photovoltaic material. J Phys Chem C 121(6):3654–3660
34. Tsai M-L, Su S-H, Chang J-K, Tsai D-S, Chen C-H, Wu C-I, Li L-J, Chen L-J, He J-H (2014) Monolayer MoS_2 heterojunction solar cells. ACS Nano 8(8):8317–8322
35. Liu H, Du Y, Deng Y, Peide DY (2015) Semiconducting black phosphorus: synthesis, transport properties and electronic applications. Chem Soc Rev 44(9):2732–2743
36. Mak KF, Shan J (2016) Photonics and optoelectronics of 2D semiconductor transition metal dichalcogenides. Nat Photonics 10(4):216
37. Ataca C, Sahin H, Ciraci S (2012) Stable, single-layer MX2 transition-metal oxides and dichalcogenides in a honeycomb-like structure. J Phys Chem C 116(16):8983–8999
38. Wilson JA, Yoffe A (1969) The transition metal dichalcogenides discussion and interpretation of the observed optical, electrical and structural properties. Adv Phys 18(73):193–335
39. Wang X, Quhe R, Cui W, Zhi Y, Huang Y, An Y, Dai X, Tang Y, Chen W, Wu Z (2018) Electric field effects on the electronic and optical properties in C_2N/Sb van der Waals heterostructure. Carbon 129:738–744
40. Husain AA, Hasan WZW, Shafie S, Hamidon MN, Pandey SS (2018) A review of transparent solar photovoltaic technologies. Renew Sustain Energy Rev 94:779–791
41. Li X-H, Wang B-J, Cai X-L, Yu W-Y, Zhu Y-Y, Li F-Y, Fan R-X, Zhang Y-S, Ke S-H (2018) Strain-tunable electronic properties and band alignments in GaTe/C_2N heterostructure: a first-principles calculation. Nanoscale Res Lett 13(1):300–310
42. Idrees M, Din H, Khan S, Ahmad I, Gan L-Y, Nguyen CV, Amin B (2019) Van der Waals heterostructures of P, BSe, and SiC monolayers. J Appl Phys 125(9):094301–094310
43. Din H, Idrees M, Albar A, Shafiq M, Ahmad I, Nguyen CV, Amin B (2019) Rashba spin splitting and photocatalytic properties of GeC-M SSe (M = Mo, W) van der Waals heterostructures. Phys Rev B 100(16):165425
44. Pham KD, Hieu NN, Bui LM, Phuc HV, Hoi BD, Tu LT, Bach LG, Ilyasov VV, Amin B, Idrees M (2019) Vertical strain and electric field tunable electronic properties of type-II band alignment C2N/InSe van der Waals heterostructure. Chem Phys Lett 716:155–161
45. Pham KD, Bach LG, Amin B, Idrees M, Hieu NN, Phuc HV, Bui H, Nguyen CV (2019) Tri-layered van der Waals heterostructures based on graphene, gallium selenide and molybdenum selenide. J Appl Phys 125(22):225304
46. Aydinli A, Gasanly N, Gökşen K (2000) Donor–acceptor pair recombination in gallium sulfide. J Appl Phys 88(12):7144–7149
47. Aulich E, Brebner J, Mooser E (1969) Indirect energy gap in GaSe and GaS. Physica Status Solidi(b) 31(1):129–131
48. Cingolani A, Minafra A, Tantalo P, Paorici C (1971) Edge emission in GaSe and GaS. physica status solidi (a) 4 (1):K83-K85
49. Chiricenco V, Caraman M, Rusu I, Leontie L (2003) On the luminescence of GaS (Cu) single crystals. J Lumin 101(1–2):71–77
50. Sameshima K, Sano T, Yamaguchi K (2016) Self-formation of ultrahigh-density (10^{12} cm^{-2}) InAs quantum dots on InAsSb/GaAs (001) and their photoluminescence properties. Appl Phys Express 9(7):075501–075506
51. Clark SJ, Segall MD, Pickard CJ, Hasnip PJ, Probert MI, Refson K, Payne MC (2005) First principles methods using CASTEP. Z Kristallogr Cryst Mater 220(5/6):567–570
52. Materials Studio simulation environment (2016) Release 2016. Accelrys Software Inc, San Diego
53. Perdew JP, Burke K, Ernzerhof M (1996) Generalized gradient approximation made simple. Phys Rev Lett 77(18):3865–3868
54. Grimme S (2006) Semiempirical GGA-type density functional constructed with a long-range dispersion correction. J Comput Chem 27(15):1787–1799
55. Goerigk L (2015) Treating London-dispersion effects with the latest Minnesota density functionals: problems and possible solutions. JPhy Chem Lett 6(19):3891–3896
56. Wang B-J, Li X-H, Zhao R, Cai X-L, Yu W-Y, Li W-B, Liu Z-S, Zhang L-W, Ke S-H (2018) Electronic structures and enhanced photocatalytic properties of blue phosphorene/BSe van der Waals heterostructures. J Mater Chem A 6(19):8923–8929

57. Paier J, Marsman M, Hummer K, Kresse G, Gerber IC, Ángyán JG (2006) Screened hybrid density functionals applied to solids. J Chem Phys 124(15):154709–154712
58. Guan Z, Ni S (2017) Insights from first principles graphene/gC_2N bilayer: gap opening, enhanced visible light response and electrical field tuning band structure. Appl Phys A 123(11):678
59. Yagmurcukardes M, Senger R, Peeters F, Sahin H (2016) Mechanical properties of monolayer GaS and GaSe crystals. Phys Rev B 94(24):245407
60. Du J, Xia C, Xiong W, Zhao X, Wang T, Jia Y (2016) Tuning the electronic structures and magnetism of two-dimensional porous C_2N via transition metal embedding. Phys Chem Chem Phys 18(32):22678–22686
61. Xu Y, Peng B, Zhang H, Shao H, Zhang R, Zhu H (2017) First-principle calculations of optical properties of monolayer arsenene and antimonene allotropes. AnP 529(4):1600152–1600169
62. Liang Z, Xu B, Xiang H, Xia Y, Yin J, Liu Z (2016) Carrier-tunable magnetism in two dimensional graphene-like C_2N. RSC Adv 6(59):54027–54031
63. Wei W, Dai Y, Niu C, Li X, Ma Y, Huang B (2015) Electronic properties of two-dimensional van der Waals GaS/GaSe heterostructures. J Mater Chem C 3(43):11548–11554
64. Zhu Y, Jain N, Mohata DK, Datta S, Lubyshev D, Fastenau JM, Liu AK, Hudait MK (2013) Band offset determination of mixed As/Sb type-II staggered gap heterostructure for n-channel tunnel field effect transistor application. J Appl Phys 113(2):024319
65. Sun J, Zhang R, Li X, Yang J (2016) A many-body GW+ BSE investigation of electronic and optical properties of C_2N. Appl Phys Lett 109(13):133108–133121
66. Shockley W, Queisser HJ (1961) Detailed balance limit of efficiency of p–n junction solar cells. J Appl Phys 32(3):510–519
67. Soref RA (1993) Silicon-based optoelectronics. Proc IEEE 81(12):1687–1706
68. Opoku F, Govender KK, van Sittert CGCE, Govender PP (2017) Role of MoS2 and WS2 monolayers on photocatalytic hydrogen production and the pollutant degradation of monoclinic BiVO 4: a first-principles study. New J Chem 41(20):11701–11713
69. Antunez PD, Buckley JJ, Brutchey RL (2011) Tin and germanium monochalcogenide IV–VI semiconductor nanocrystals for use in solar cells. Nanoscale 3(6):2399–2411
70. Wehenkel DJ, Hendriks KH, Wienk MM, Janssen RA (2012) The effect of bias light on the spectral responsivity of organic solar cells. Org Electron 13(12):3284–3290
71. Yuan L-D, Deng H-X, Li S-S, Wei S-H, Luo J-W (2018) Unified theory of direct or indirect band-gap nature of conventional semiconductors. Phys Rev B 98(24):245203–245218
72. Opoku F, Govender KK, van Sittert CGCE, Govender PP (2017) Understanding the mechanism of enhanced charge separation and visible light photocatalytic activity of modified wurtzite ZnO with nanoclusters of ZnS and graphene oxide: from a hybrid density functional study. New J Chem 41(16):8140–8155
73. Peng X, Tang F, Copple A (2012) Engineering the work function of armchair graphene nanoribbons using strain and functional species: a first principles study. J Phys Condens Matter 24(7):075501–075527
74. Yagmurcukardes M, Senger R, Peeters F, Sahin H (2016) Mechanical properties of monolayer GaS and GaSe crystals. Phys Rev B 94(24):245407–245414
75. Xu W, Chen C, Tang C, Li Y, Xu L (2018) Design of boron doped C2N–C3N coplanar conjugated heterostructure for efficient HER electrocatalysis. Sci Rep 8(1):5570–5661
76. Tan X, Kou L, Tahini HA, Smith SC (2015) Conductive graphitic carbon nitride as an ideal material for electrocatalytically switchable CO_2 Capture. Sci Rep 5:17636
77. Alam KM, Kumar P, Kar P, Thakur UK, Zeng S, Cui K, Shankar K (2019) Enhanced charge separation in g-C_3N_4–BiOI heterostructures for visible light driven photoelectrochemical water splitting. Nanoscale Adv 1:1460–1471
78. Zeng F, Huang W-Q, Xiao J-H, Li Y-y, Peng W, Hu W, Li K, Huang G-F (2018) Isotype heterojunction g-C_3N_4/g-C_3N_4 nanosheets as 2D support to highly dispersed 0D metal oxide nanoparticles: generalized self-assembly and its high photocatalytic activity. J Phys D Appl Phys 52(2):25501–25529
79. Wu H-Y, Yang K, Si Y, Huang W-Q, Hu W, Peng P, Huang G-F (2018) Interfacial interaction between Boron cluster and metal oxide surface and its effects: a case study of B_{20}/Ag_3PO_4 van der Waals Heterostructure. J Phys Chem C 122(11):6151–6158
80. Shen Q, Ogomi Y, Chang J, Toyoda T, Fujiwara K, Yoshino K, Sato K, Yamazaki K, Akimoto M, Kuga Y (2015) Optical absorption, charge separation and recombination dynamics in Sn/Pb cocktail perovskite solar cells and their relationships to photovoltaic performances. J Mater Chem A 3(17):9308–9316
81. Kang X, Liu S, Dai Z, He Y, Song X, Tan Z (2019) Titanium dioxide: from engineering to applications. Catalysts 9(2):191–223
82. Pearson RG (1988) Absolute electronegativity and hardness: application to inorganic chemistry. Inorg Chem 27(4):734–740
83. Jia X, Cao J, Lin H, Zhang M, Guo X, Chen S (2017) Transforming type-I to type-II heterostructure photocatalyst via energy band engineering: a case study of I-BiOCl/I-BiOBr. Appl Catal B 204:505–514
84. Höcker J, Kiermasch D, Rieder P, Tvingstedt K, Baumann A, Dyakonov V (2019) Efficient solution processed $CH_3NH_3PbI_3$ perovskite solar cells with polyTPD hole transport layer. Z Naturforschung A 74(8):665–672
85. Subrahmanyam A, Mahendra K, Kulshreshtha A (1979) Theoretical consideration of curve fill factor in solar cells. In: Solar energy for rural development, pp 474–477
86. Herguth A (2017) On the meaning (fullness) of the intensity unit 'suns' in light induced degradation experiments. Energy Procedia 124(2017):53–59